

Article

## Combined Pharmacophore Modeling, 3D-QSAR, Homology Modeling and Docking Studies on CYP11B1 Inhibitors

Rui Yu <sup>1</sup>, Juan Wang <sup>2</sup>, Rui Wang <sup>1</sup>, Yong Lin <sup>3</sup>, Yong Hu <sup>1</sup>, Yuanqiang Wang <sup>1</sup>, Mao Shu <sup>1,\*</sup> and Zhihua Lin <sup>1,4,\*</sup>

<sup>1</sup> School of Pharmacy and Bioengineering, Chongqing University of Technology, Chongqing 400054, China; E-Mails: 379490507@163.com (R.Y.); wangrx1022@163.com (R.W.); huy@cqut.edu.cn (Y.H.); wangyqnn@cqut.edu.cn (Y.W.)

<sup>2</sup> College of Bioengineering, Chongqing University, Chongqing 400044, China; E-Mail: wangjuan7986@126.com

<sup>3</sup> School of Chemistry and Chemical Engineering, Chongqing University of Technology, Chongqing 400054, China; E-Mail: linyong@cqut.edu.cn

<sup>4</sup> School of Chemistry and Chemical Engineering, Chongqing University, Chongqing 400044, China

\* Authors to whom correspondence should be addressed; E-Mails: sm7507@126.com (M.S.); zhlin@cqut.edu.cn (Z.L.); Tel./Fax: +86-23-62563182 (M.S.).

Academic Editor: Iwao Ojima

Received: 11 September 2014 / Accepted: 29 November 2014 / Published: 9 January 2015

---

**Abstract:** The mitochondrial cytochrome P450 enzymes inhibitor steroid 11 $\beta$ -hydroxylase (CYP11B1) can decrease the production of cortisol. Therefore, these inhibitors have an effect in the treatment of Cushing's syndrome. A pharmacophore model generated by Genetic Algorithm with Linear Assignment for Hypermolecular Alignment of Datasets (GALAHAD) was used to align the compounds and perform comparative molecular field analysis (CoMFA) with  $Q^2 = 0.658$ ,  $R^2 = 0.959$ . The pharmacophore model contained six hydrophobic regions and one acceptor atom, and electropositive and bulky substituents would be tolerated at the A and B sites, respectively. A three-dimensional quantitative structure-activity relationship (3D-QSAR) study based on the alignment with the atom root mean square (RMS) was applied using comparative molecular field analysis (CoMFA) with  $Q^2 = 0.666$ ,  $R^2 = 0.978$ , and comparative molecular similarity indices analysis (CoMSIA) with  $Q^2 = 0.721$ ,  $R^2 = 0.972$ . These results proved that all the models have good predictability of the bioactivities of inhibitors. Furthermore, the QSAR models indicated that a hydrogen bond acceptor substituent would be disfavored at the A and B groups,

while hydrophobic groups would be favored at the B site. The three-dimensional (3D) model of the CYP11B1 was generated based on the crystal structure of the CYP11B2 (PDB code 4DVQ). In order to probe the ligand-binding modes, Surflex-dock was employed to dock CYP11B1 inhibitory compounds into the active site of the receptor. The docking result showed that the imidazolidine ring of CYP11B1 inhibitors form H bonds with the amino group of residue Arg155 and Arg519, which suggested that an electronegative substituent at these positions could enhance the activities of compounds. All the models generated by GALAHAD QSAR and Docking methods provide guidance about how to design novel and potential drugs for Cushing's syndrome treatment.

**Keywords:** CYP11B1 inhibitors; 3D-QSAR; pharmacophore model; Cushing's syndrome

---

## 1. Introduction

Cortisol is a principal glucocorticoid [1] that is not only used in the treatment of inflammation, allergy, collagen diseases, asthma, adrenocortical deficiency, shock, and some neoplastic conditions, but also exhibits many physiological functions in the regulation of metabolism of life substances, blood pressure and cardiovascular function [2]. Biosynthesis of cortisol take place in the adrenal cortex whose final step (conversion from 11-deoxycortisol) is catalyzed by the mitochondrial cytochrome P450 enzyme steroid 11 $\beta$ -hydroxylase (CYP11B1) [1,3]. (Please reorder references numbers, you jumped 2 and 3 before 4)

The secretion of cortisol is precisely controlled by adrenocorticotrophic hormone (ACTH) [2,4,5] within the negative feedback cycle of hypothalamic-pituitary-adrenal axis [1]. However, pathological changes in adrenals and the upstream regulating switches can cause an overproduction of cortisol, which is known as Cushing's syndrome. Cushing's syndrome patients mainly show a "moon face", sanguine temperament appearance, obesity, acne, purple lines, high blood pressure, secondary diabetes and osteoporosis, *etc.* It's a hormonal disorder caused by prolonged exposure to high levels of circulating glucocorticoids such as cortisol [6,7].

Normally, the surgical removal of adrenal or pituitary tumors is used for the treatment of hypercortisolism [8]. However, as mentioned above, CYP11B1 can promote the synthesis of cortisol. Therefore, inhibition of CYP11B1 as the pharmacological approach to block cortisol biosynthesis represents a treatment for Cushing's syndrome [9]. Inhibitors of cortisol biosynthesis, such as ketoconazole, etomidate, and metyrapone have been used in the clinic [4], however, all of them show severe side effects due to the fact that they are unselective. Metyrapone is the only drug reported to be a relatively selective CYP11B1 inhibitor.

In recent years, a series of mitochondrial cytochrome P450 (CYP) superfamily receptors [10], such as CYP1A2, CYP17, CYP19, CYP11B2 [7,11,12], were used to analysis the combination of ligand compounds in different molecular docking studies [13]. Few studies published so far have used the pharmacophore modeling or 3D-QSAR approaches for modeling ligand interactions with the CYP11B1 receptor [14]. In addition, a three-dimensional model of CYP11B1 has not been published yet. Therefore, in the present study we aimed to build and validate homology models of CYP11B1 [15]

and then run a docking procedure which indicates the active groups and atoms of inhibitory compounds. In order to analyse the molecular shape of CYP11B1 inhibitors [14], a series of compounds with good inhibitory activities synthesized by Hartmann [15] were collected to establish 3D-QSAR models using CoMFA and CoMSIA. The combination of the pharmacophore model [16] GALAHAD and CoMFA methods also helped establish the structure-activity relationship (SAR) of CYP11B1 inhibitors [17].

## 2. Results and Discussion

### 2.1. GALAHAD Modeling Results

Once GALAHAD modeling based on the training set compounds was completed (Figure 1a), a total of 20 pharmacophore models were generated using common feature hypothesis generation approach. The generated pharmacophore model contained six hydrophobic regions and one acceptor atom (Figure 1b).

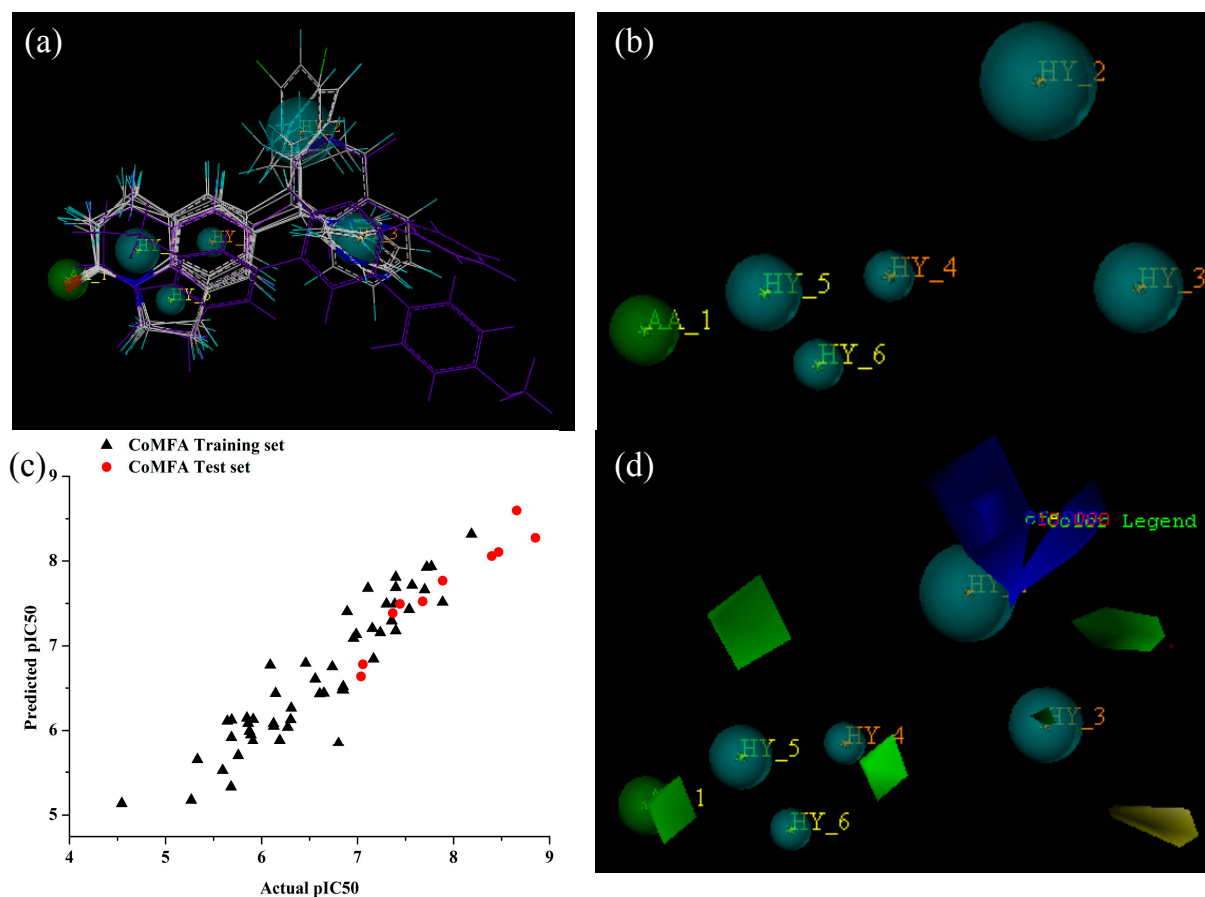


**Figure 1.** The results generated using GALAHAD modeling method. (a) The alignment of 62 CYP11B1 inhibitors; (b) The best pharmacophore model generated by the GALAHAD method; (c) Observed *versus* predicted pIC<sub>50</sub> values derived from CoMFA of both training and test sets; (d) CoMFA contour maps for the best pharmacophore model.

They are featured as the cyan balls and the green ball, respectively [18,19]. According to the principals, if all energy parameters had the same level, the Pareto rank would be taken into consideration. Thus, model 1 with a Pareto rank of 0 was selected as the best template to do the CoMFA analysis. The result of this model is  $Q^2 = 0.658$ ,  $R^2 = 0.959$ ,  $F = 82.102$ ,  $SEE = 0.154$  and had two components. The model obtained from combined method had an acceptable balance between energy, pharmacophoric coherence and pharmacosteric overlap statistically. Therefore model 1 was used as the template in aligning the full dataset and did partial least square (PLS) analysis [20,21]. The contour plots between observed and predicted activities of all compounds were shown in Table 1. Nearly, all of compounds were located on the trend line (Figure 1c), indicating that the proposed model was able to successfully predict compounds in test set. In the CoMFA study, the contour maps (Figure 1d) of the pharmacophore model indicated that the blue and yellow contours located around site A would be electropositive groups. The yellow contours located at the B site around the hydrophobe group indicated that a bulky substituent would not be tolerated. The green contours around acceptor atoms and hydrophobe groups indicated that a bulky substituent would be tolerated.

**Table 1.** The observed and predicted activities of 62 CYP11B1 inhibitors generated from different modeling methods.

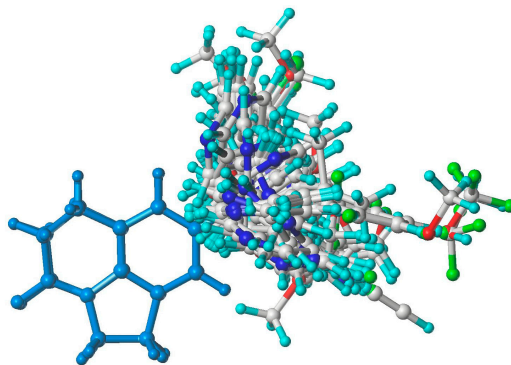
Compounds	pIC <sub>50</sub>			
	Observed	Predicted		
		Pharmacophore		RMS
		CoMFA	CoMFA	CoMSIA
1	6.460	6.795	6.503	6.267
2	6.650	6.442	6.724	6.837
3	5.910	5.872	6.383	7.355
4	6.854	6.476	6.216	6.870
5	5.848	6.147	7.039	6.978
6	6.128	6.049	6.027	5.972
7	5.268	5.174	5.294	5.237
8	6.559	6.608	6.635	6.589
9	5.595	5.521	5.605	5.488
10	6.092	6.773	6.594	6.809
11	6.274	6.038	6.286	6.199
12	7.056	6.781	7.047	7.100
13	6.190	5.883	5.569	5.832
14	7.036	6.638	7.112	7.184
15	5.874	5.991	5.820	5.838
16	6.125	6.082	6.059	6.145
17	7.387	7.493	7.384	7.462
18	8.398	8.059	8.256	8.199
19	7.167	6.846	6.657	6.474
20	5.644	6.111	5.710	5.526
21	5.914	6.131	6.081	6.216
22	7.444	7.493	7.465	7.332
23	7.108	7.679	7.499	7.460
24	7.770	7.936	8.755	8.459
25	8.187	8.317	8.456	8.444

Table 1. Cont.

Compounds	pIC <sub>50</sub>			
	Observed	Predicted		
		Pharmacophore		RMS
		CoMFA	CoMFA	CoMSIA
26	8.854	8.274	8.730	8.643
27	8.658	8.598	8.663	8.569
28	8.469	8.105	8.332	8.414
29	7.721	7.929	7.230	8.223
30	7.398	7.690	7.280	7.521
31	7.538	7.430	7.158	7.394
32	7.569	7.715	7.188	7.315
33	6.959	7.089	7.352	7.539
34	7.398	7.810	6.608	7.151
35	6.842	6.483	7.030	7.225
36	7.155	7.205	7.335	7.278
37	7.301	7.494	7.316	7.284
38	7.699	7.662	7.777	7.700
39	7.886	7.515	7.693	7.596
40	6.146	6.438	5.974	6.149
41	6.607	6.435	6.367	6.426
42	6.801	5.847	6.021	6.082
43	6.987	7.134	7.057	6.944
44	5.689	6.125	5.698	5.658
45	5.890	5.949	5.699	6.199
46	6.851	6.518	6.369	7.034
47	7.886	7.768	6.820	6.869
48	4.544	5.135	5.004	4.603
49	5.683	5.329	5.408	5.758
50	7.237	7.156	7.095	7.108
51	7.367	7.385	7.244	7.113
52	6.310	6.264	6.075	6.183
53	7.398	7.178	7.525	7.237
54	6.738	6.753	6.844	6.712
55	6.305	6.128	6.510	6.321
56	5.757	5.695	5.681	5.796
57	6.893	7.405	7.022	7.331
58	5.862	6.085	6.465	7.034
59	7.678	7.524	7.821	7.828
60	7.357	7.294	6.605	6.842
61	5.687	5.917	5.705	5.600
62	5.333	5.648	5.336	5.397

## 2.2. 3D-QSAR Modeling Result

The superimposition of all molecules aligned with a common substructure is shown in Figure 2. The aligned molecules were used to generate CoMFA and CoMSIA models which were developed using a combination of different fields, and the statistically significant models were reported with statistical parameters shown in Table 2.



**Figure 2.** Molecular alignment based on atom root mean square (RMS) was used in the 3D-QSAR studies.

**Table 2.** Summary of validation statistics for CoMFA and CoMSIA Models generated based on the RMS.

Method	Q <sup>2</sup>	R <sup>2</sup>	N	SEE	F
CoMFA + SE	0.666	0.978	6	0.159	270.441
CoMSIA + S	0.510	0.833	6	0.441	29.904
CoMSIA + E	0.416	0.869	5	0.385	49.217
CoMSIA + H	0.446	0.852	6	0.414	34.641
CoMSIA + D	-	-	-	-	-
CoMSIA + A	0.219	0.729	6	0.562	16.074
CoMSIA + SE	0.531	0.955	6	0.229	126.791
CoMSIA + SH	0.626	0.890	6	0.357	48.766
CoMSIA + SA	0.487	0.830	6	0.445	29.213
CoMSIA + EH	0.446	0.882	6	0.361	70.933
CoMSIA + EA	0.520	0.924	6	0.298	72.500
CoMSIA + HA	0.443	0.873	6	0.384	41.344
CoMSIA + SEH	0.547	0.912	6	0.312	98.306
CoMSIA + SEA	0.699	0.962	6	0.211	150.046
CoMSIA + SHA	0.595	0.916	6	0.312	65.746
CoMSIA + EHA	0.632	0.958	6	0.220	138.387
CoMSIA + SEHA	0.721	0.972	6	0.180	209.908

The CoMFA model using both steric and electrostatic fields gave Q<sup>2</sup> of 0.666, R<sup>2</sup> of 0.978, F of 270.441 and SEE of 0.159 values with six components. In the CoMSIA study, the first five models using a single field indicated that the steric field is the most important one. The combination of the steric, electrostatic, hydrophobic, and electrostatic fields led to the S + E + H + A model (Q<sup>2</sup> = 0.721, N = 6), providing the best overall model. The best model led to the highest R<sup>2</sup>, F and the lowest SEE

( $R^2 = 0.972$ ,  $F = 209.908$  and  $SEE = 0.180$ ). For these reasons, we considered S+E+H+A to be the best possible combination.

### 2.3. Predictive Power of 3D-QSAR Analyses

CoMFA and CoMSIA analysis developed QSAR models using the training set of CYP11B1 inhibitors. The predicted and observed activities of these compounds were obtained by using the best model that was given in Table 1. The contour plots between observed and predicted bioactivities of training and test set were shown in Figure 3. Most of compounds were located near the trend line, implying the proposed model is able to successfully predict the activities of compounds, which indicated that these 3D-QSAR models are reliable and powerful in predicting  $pIC_{50}$  values.

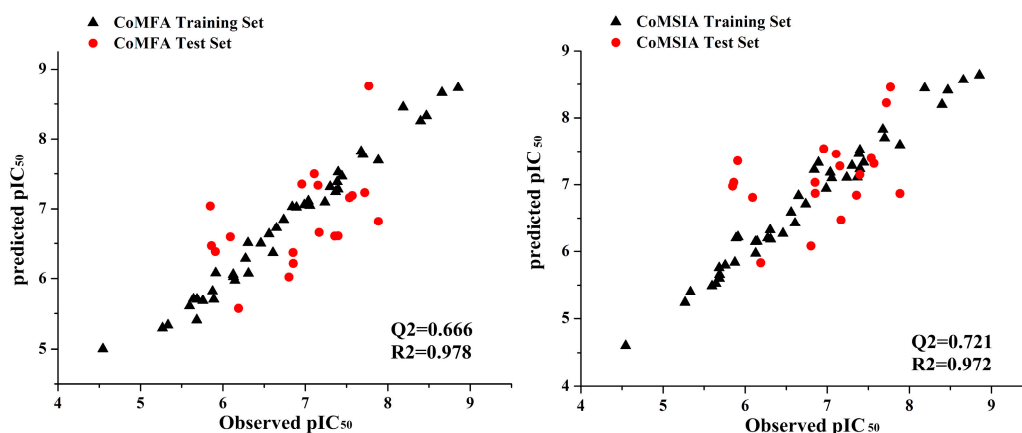


**Figure 3.** Observed *versus* predicted  $pIC_{50}$  values of both training and test sets using CoMFA and CoMSIA in 3D-QSAR mode.

The 3D contour maps were generated to represent the 3D-QSAR results produced by the CoMFA and CoMSIA methods. The different field contributions of CoMFA and CoMSIA models were illustrated with compound **26** (Figure 4). The results indicated that most of the contours were located at the right side of the compound structures (A and B groups). In the CoMFA model, the contributions of the steric and electrostatic fields to activity were 40.9% and 59.1%. The yellow and blue contours located at the A site indicated that a bulky substituent would not be tolerated and electropositive groups would be favorable [22]. However, bulky substituents and electropositive groups would not be favorable to the B group (Figure 4a) [23]. In the CoMSIA model, the contributions of the steric, electrostatic, hydrophobic and acceptor fields were 13.2%, 40.7%, 22.0% and 24.2%, respectively. The percentages of different fields indicated that the steric and electrostatic fields almost make the same contribution. The combination of these four fields provided the most predictive model for CYP11B1 inhibitors, and the electrostatic field was the most significant for bioactivity prediction. The contour maps of the steric and electrostatic fields of CoMSIA (Figure 4b) were generally in accordance with the field distribution of the CoMFA maps (Figure 4a). The hydrophobic and hydrogen bond acceptor field contour maps of CoMSIA implied that hydrogen bond acceptor substituents were disfavored at the A and B sites, while, hydrophobic groups were favored at the B site (Figure 4c) [24]. The small and electropositive substituent such as an aliphatic amine group would be tolerated at the A site. Small, electronegative and hydrophobic substituent such as trifluoromethanesulfonamide group would be tolerated at B site.

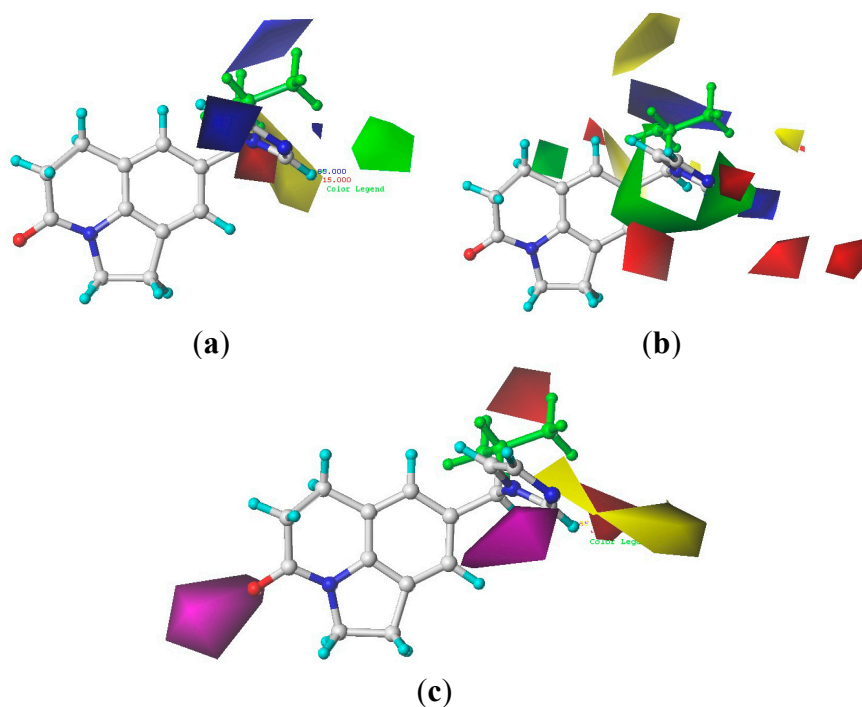


**Figure 4.** CoMFA and CoMSIA contour maps displayed using the most potent compound **26**. (a) CoMFA steric and electrostatic contour map (green indicates favored, yellow indicates disfavored, blue indicate favored, red indicates disfavored); (b) CoMSIA steric and electrostatic contour map (green indicates favored, yellow indicates disfavored, blue indicates favored, red indicates disfavored); (c) CoMSIA hydrophobic and acceptor contour map (yellow indicates favored, white indicates disfavored, magenta indicates favored, red indicates disfavored).

#### 2.4. Homology Modeling Result

The length of the CYP11B1 sequence was 574 aa and the most suitable template was the A chain of the CYP11B2 protein (PDB code: 4DVQ). The BLASTP alignment between the CYP11B2 template and CYP11B1 sequences is shown in Figure 5a, revealing 81% identity and 95% consensus similarity. Then, after the structural-based alignment of CYP11B1 from 4DVQ-A, the initial 3D structure of CYP11B1 was obtained from a homology modeling procedure shown in Figure 5d. Evaluation of the homology models consists of Profiles\_3D scores and Ramachandran plot analysis [25] (Figure 5c).

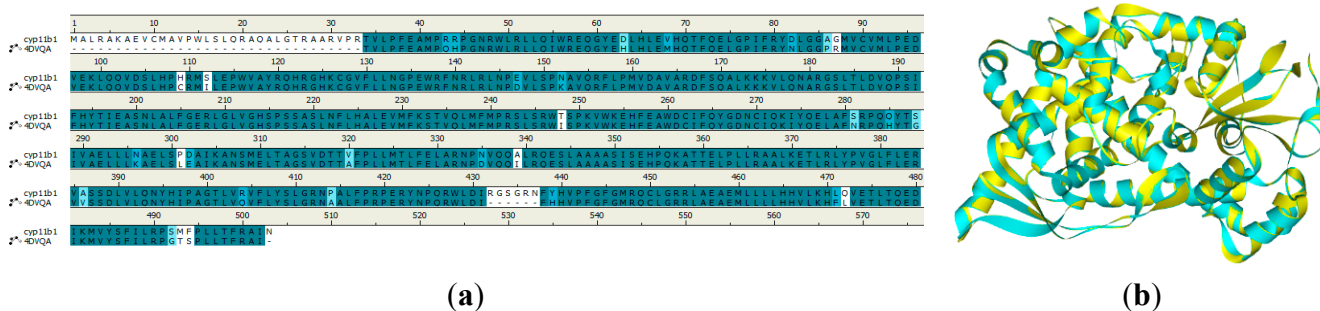


**Figure 5.** Cont.



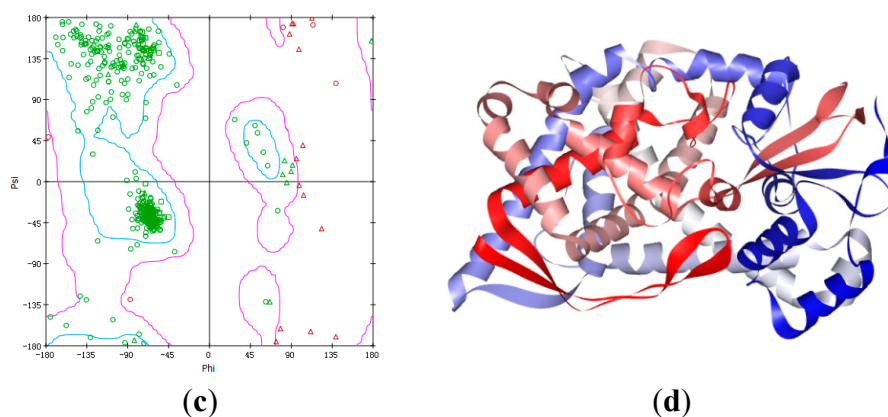


**Figure 5.** Structural-based alignment of CYP11B1 and the template PDB ID: 4DVQ-A. (a) The sequence shaded in cyan represents sequence similarity; (b) Superposition of the predicted CYP11B1 model onto the template PDB ID: 4DVQ-A, yellow indicates template, blue indicates predicted model; (c) Ramachandran Plot of the best CYP11B1 model; (d) Structure of the best predicted model.

Profiles\_3D scores shown in the Ramachandran Plot of the CYP11B1 model showed a good distribution of 574 amino acid residues of CYP11B1. About 97.0% of the residues featured with green plots were most favored and an additionally allowed region, and only 3.0% residues featured with red plots were an erroneously allowed region.

### 2.5. Docking Analysis

Sixty two (62) CYP11B1 inhibitors were evaluated by docking scores after Surflex-dock. According to the rule, compounds with scores above 7 were considered as active in the docking study. In this paper compounds **33** and **37** scored 7.8544 and 7.1932 (Figure 6a,b) and showed a similar docking mode in the active site of the receptor. The binding cavity of CYP11B1 is formed by residues Arg155, Phe175, Arg519, Cys521, Leu522. Hydrogen atoms of the amino group of residue Arg155 and Arg519 are found near N3 of the imidazolidine ring, thus suggesting that electronegative substituents at these positions could enhance the activities of compounds binding to CYP11B1 [26,27].

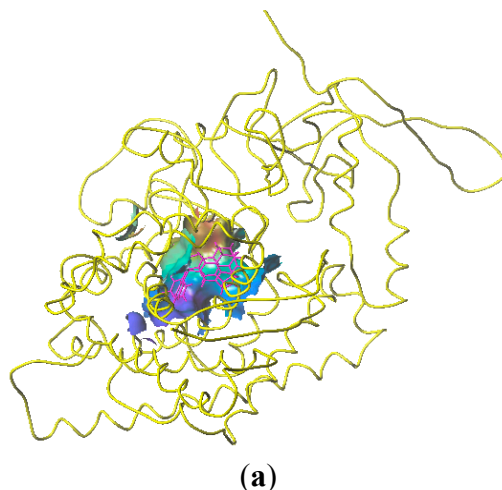


**Figure 6.** Cont.



Table 3. The structures and bioactivity values of active compounds.

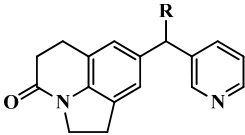
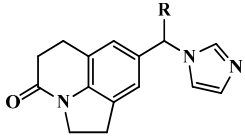
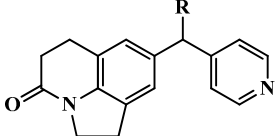
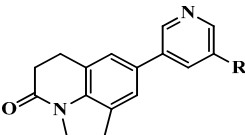
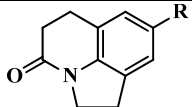
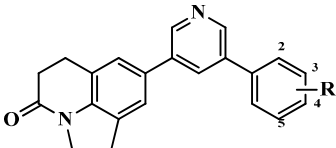
Compound	Skeleton	R	IC <sub>50</sub> (nM)	pIC <sub>50</sub>
1		OH	347	6.4597
2		H	224	6.6498
3 *		=CH <sub>2</sub>	1230	5.9101
4 *		Me	140	6.8539
5 *		<i>i</i> -Pr	1420	5.8477
6		Ph	745	6.1278
7		Ph,OH	5399	5.2677
8		2-MeOPh	276	6.5591
9		3-MeOPh	2539	5.5953
10 *		4-MeOPh	810	6.0915
11		3-FPh	532	6.2741
12 #		4-FPh	88	7.0555
13 *		3-ClPh	646	6.1898
14 #		4-ClPh	92	7.0362
15		3-CH <sub>3</sub> Ph	1336	5.8742
16			OH	750
17		=CH <sub>2</sub>	41	7.3872
18 #		Me	4	8.3979
19 *		Ph	68	7.1675
20		2-MeOPh	2270	5.6440
21 *		3-MePh	1220	5.9136
22 #		3-ClPh	36	7.4437
23 *		4-FPh	78	7.1079
24 *			Me	17
25		Et	6.5	8.1871
26 #		<i>i</i> -propyl	1.4	8.8539
27 #		<i>c</i> -propyl	2.2	8.6576
28 #		<i>c</i> -butyl	3.4	8.4685
29 *		=CH <sub>2</sub>	19	7.7212
30 *		2-FPh	40	7.3979
31 *		3-FPh	29	7.5376
32 *		4-FPh	27	7.5686
33 *		3-MeOPh	110	6.9586
34 *		4-MeOPh	40	7.3979
35		3-CNPh	144	6.8416
36 *		4-CNPh	70	7.1549
37		Ph	50	7.3010
38		2-furanyl	20	7.6990
39		2-thienyl	13	7.8861
40		H	715	6.1457
41		OMe	247	6.6073
42 *		OEt	158	6.8013
43		O <i>i</i> Pr	103	6.9872
44		OH	2045	5.6893
45		F	1288	5.8901
46		CF <sub>3</sub>	141	6.8508

Table 3. Cont.

Compound	Skeleton	R	IC <sub>50</sub> (nM)	pIC <sub>50</sub>
47 #*		4-isoquinoline	13	7.8861
48		5-pyrimidine	28546	4.5445
49		1-imidazole	2077	5.6826
50		H	58	7.2366
51 #		2-F	43	7.3665
52		3-F	490	6.3098
53		4-F	40	7.3979
54		2,5-F	183	6.7375
55		3,4-F	496	6.3045
56		3,5-F	1748	5.7575
57		2-OMe	128	6.8928
58 *		3-OMe	1374	5.8620
59 #		4-OMe	21	7.6778
60 *		3-OH	44	7.3565
61		3-OCF <sub>3</sub>	2058	5.6866
62		3-CF <sub>3</sub>	4646	5.3329

Molecules marked with \*: belong to the test set of 3D-QSAR method; Molecules marked with #: belong to the test set of GALAHAD method.

### 3.3. 3D-QSAR Modeling

The structures of CYP11B1 inhibitors used for the 3D-QSAR study were randomly divided into a training set (42 molecules) and a test set (20 molecules) [34] (Table 1). All structures were energy minimized using the Powell gradient algorithm under the Tripos force field with Gasteiger-Marsili atomic partial charges. The most potent CYP11B1 inhibitor (compound **26**) was selected as the alignment template (Figure 7), which was also used as template to build all the other inhibitors with the atom root mean square (RMS) approach.

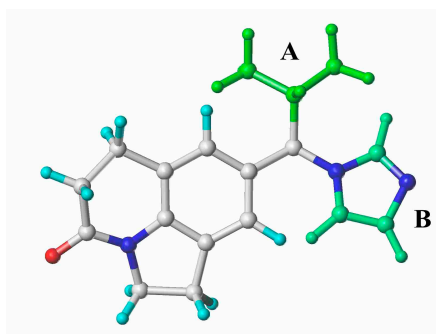


**Figure 7.** The compound with the highest activity of CYP11B1 inhibition (compound **26**) combined with A and B groups.

3D-QSAR models were constructed by using CoMFA and CoMSIA methods based on the molecular alignment. The default values of the parameters of the CoMFA and CoMSIA methods were used. The CoMFA method was performed using steric and electrostatic fields with standard 30 kcal/mol cutoffs. In the CoMSIA study, besides steric and electrostatic fields, three other different fields were

calculated: hydrophobic, hydrogen bond donor, and hydrogen bond acceptor [34–36]. A series of models were constructed with an increasing number of partial least squares (PLS) analysis factors. The numbers of components in the PLS models were optimized by using the cross-validated correlation coefficient ( $Q^2$ ), non-cross-validated correlation coefficient ( $R^2$ ), standard error estimate (SEE) and F-statistic values (F), *etc.*, which were obtained from the leave-one-out (LOO) cross-validation procedures [37,38]. According these parameters, the best model was chosen to predict bioactivities of compounds. In this work the best 3D-QSAR model was graphically represented by field contour maps, and the coefficients were generated using the StDev/Coeff field type.

### 3.4. Homology Modeling and Docking Analysis

The amino acid sequence of CYP11B1 (GenBank: AAH96285.1) was obtained from the National Center for Biotechnology Information Database (NCBI)[39]. Identification of candidate templates was performed by sequence similarity search using BLAST search (NCBI Server) protocol with default values and each target was searched and downloaded from the NCBI database. The CYP11B1 sequence was aligned to the templates and homology models of CYP11B1 built with the default parameters. Subsequently, the models were analyzed based on Profiles\_3D scores and Ramachandran plots which indicate the percentage of amino acids located in the disallowed regions. The interaction of small molecule ligands with a protein, which implied atomic-detail accuracy including position and conformation, was obtained from the docking procedure. Docking and scoring were performed using the Sybyl-X2.1 software (Tripos Inc., St. Louis, MO, USA, 2014) Surflex-Dock method. The docking receptor CYP11B1 was constructed as described in Homology modeling, while the ligands set consisted of all 62 inhibitors. Polar hydrogen atoms were added to both protein and ligand structures. The other parameters of Surflex-Dock methods were used as default values. The best docking pose was selected according to the total score.

## 4. Conclusions

CYP11B1 plays a crucial role in the biosynthesis of cortisol which can cause a series of diseases known as Cushing's syndrome. Therefore, CYP11B1 inhibitors that can be regarded as a pharmacological approach to block cortisol biosynthesis have become another treatment for Cushing's syndrome. GALAHAD is a novel pharmacophore screening module, which generates models to analyse the pharmacophore features of ligands. A CoMFA study based on the pharmacophore (GALAHAD) alignment has been developed to derive the structure-activity relationships, which also indicate the interaction between CoMFA fields and pharmacophore features of ligands.

In this study, CoMFA and CoMSIA models were built using the alignment based on the atom root mean square (RMS), which explored the structure-activity relationship of the CYP11B1 inhibitors. These models with excellent consistency manifested good predictive ability for the test compounds. The contour maps also identified the important features contributing to interactions between the different fields and the active site of CYP11B1 inhibitors.

Homology modeling method was used to construct a 3D model of the CYP11B1 protein. Then, the Surflex-Dock analysis was used to evaluate the binding activities between the protein and ligand

compounds. The binding site indicated the interaction and combination between ligand groups and amino acid residues, which acted as a guide in the prediction and design of CYP11B1 inhibitors.

The combined pharmacophore modeling and 3D-QSAR modeling methods indicated that small and electropositive substituents would be tolerated at the A site. Meanwhile, small, electronegative and hydrophobic substituents would be better at the B site. The docking results indicated that electronegative substituents at the B position could enhance the activities of compounds binding to CYP11B1.

### Acknowledgments

This study was supported by the National Natural Science Foundation of China (81171508, 31170747), Key Project of Natural Science Foundation of Chong Qing (CSTC 2013JJB10004), Natural Science Foundation project of Chongqing (CSTC 2010BB5304), and Science and Technology project of Chongqing Education Commission (KJ130809), Graduate Innovation Foundation of Chongqing University of Technology (YCX2013221).

### Author Contributions

M.S., Z.L. and R.Y. designed research; R.W., Y.L., Y.H. and Y.W. performed research and analyzed the data; J.W. and R.Y. wrote the paper. All authors read and approved the final manuscript.

### Conflicts of Interest

The authors declare no conflict of interest.

### References

1. Yin, L.; Lucas, S.; Maurer, F.; Kazmaier, U.; Hu, Q.; Hartmann, R.W. Novel imidazol-1-ylmethyl substituted 1,2,5,6-tetrahydropyrrolo[3,2,1-ij]quinolin-4-ones as potent and selective CYP11B1 inhibitors for the treatment of Cushing's syndrome. *J. Med. Chem.* **2012**, *55*, 6629–6633.
2. Emmerich, J.; Hu, Q.; Hanke, N.; Hartmann, R.W. Cushing's syndrome: Development of highly potent and selective CYP11B1 inhibitors of the (pyridylmethyl)pyridine type. *J. Med. Chem.* **2013**, *56*, 6022–6032.
3. Hille, U.E.; Zimmer, C.; Haupenthal, J.; Hartmann, R.W. Optimization of the First Selective Steroid-11 $\beta$ -hydroxylase (CYP11B1) Inhibitors for the Treatment of Cortisol Dependent Diseases. *ACS Med. Chem. Lett.* **2011**, *2*, 559–564.
4. White, P.C.; Rainey, W.E. Editorial: Polymorphisms in CYP11B genes and 11-hydroxylase activity. *J. Clin. Endocrinol. Metab.* **2005**, *90*, 1252–1255.
5. Hofland, J.; Hofland, L.J.; van Koetsveld, P.M.; Steenbergen, J.; de Herder, W.W.; van Eijck, C.H.; de Krijger, R.R.; van Nederveen, F.H.; van Aken, M.O.; de Groot, J.W.; *et al.* ACTH-independent macronodular adrenocortical hyperplasia reveals prevalent aberrant *in vivo* and *in vitro* responses to hormonal stimuli and coupling of arginine-vasopressin type 1a receptor to 11 $\beta$ -hydroxylase. *Orphanet J. Rare Dis.* **2013**, *8*, doi:10.1186/1750-1172-8-142.
6. Bista, B.; Beck, N. Cushing syndrome. *Indian J. Pediatr.* **2014**, *81*, 158–164.

7. Cao, C.; Yang, X.; Li, L.; Sun, R.; Xian, Y.; Lv, W.; Jing, W.; Jun, X.; Yan, G. Increased expression of CYP17 and CYP11B1 in subclinical Cushing's syndrome due to adrenal adenomas. *Int. J. Urol.* **2011**, *18*, 691–696.
8. Maser-Gluth, C.; Reincke, M.; Allolio, B.; Schulze, E. Metabolism of glucocorticoids and mineralocorticoids in patients with adrenal incidentalomas. *Eur. J. Clin. Investig.* **2000**, *30* (Suppl. 3), 83–86.
9. Hu, Q.; Yin, L.; Hartmann, R.W. Aldosterone Synthase Inhibitors as Promising Treatments for Mineralocorticoid Dependent Cardiovascular and Renal Diseases. *J. Med. Chem.* **2014**, *57*, 5011–5022.
10. Chauhan, K.; Singh, P.; Kumar, V.; Shukla, P.K.; Siddiqi, M.I.; Chauhan, P.M. Investigation of Ugi-4CC derived 1*H*-tetrazol-5-yl-(aryl) methyl piperazinyl-6-fluoro-4-oxo-1,4-dihydroquinoline-3-carboxylic acid: Synthesis, Biology and 3D-QSAR analysis. *Eur. J. Med. Chem.* **2014**, *78*, 442–454.
11. Shepphird, J.K.; Clark, R.D. A marriage made in torsional space: Using GALAHAD models to drive pharmacophore multiplet searches. *J. Comput.-Aided Mol. Des.* **2006**, *20*, 763–771.
12. Lucas, S.; Negri, M.; Heim, R.; Zimmer, C.; Hartmann, R.W. Fine-tuning the selectivity of aldosterone synthase inhibitors: Structure-activity and structure-selectivity insights from studies of heteroaryl substituted 1,2,5,6-tetrahydropyrrolo[3,2,1-ij]quinolin-4-one derivatives. *J. Med. Chem.* **2011**, *54*, 2307–2319.
13. Platania, C.B.; Salomone, S.; Leggio, G.M.; Drago, F.; Bucolo, C. Homology modeling of dopamine D2 and D3 receptors: Molecular dynamics refinement and docking evaluation. *PLoS One* **2012**, *7*, e44316.
14. Roy, P.P.; Roy, K. Exploring QSAR for CYP11B2 binding affinity and CYP11B2/CYP11B1 selectivity of diverse functional compounds using GFA and G/PLS techniques. *J. Enzym. Inhib. Med. Chem.* **2010**, *25*, 354–369.
15. Abbaszadegan, M.R.; Hassani, S.; Vakili, R.; Saberi, M.R.; Baradaran-Heravi, A.; A'Rabi, A.; Hashemipour, M.; Razzaghi-Azar, M.; Moaven, O.; Baratian, A.; *et al.* Two novel mutations in CYP11B1 and modeling the consequent alterations of the translated protein in classic congenital adrenal hyperplasia patients. *Endocrine* **2013**, *44*, 212–219.
16. Lucas, S.; Heim, R.; Negri, M.; Antes, I.; Ries, C.; Schewe, K.E.; Bisi, A.; Gobbi, S.; Hartmann, R.W. Novel aldosterone synthase inhibitors with extended carbocyclic skeleton by a combined ligand-based and structure-based drug design approach. *J. Med. Chem.* **2008**, *51*, 6138–6149.
17. Ji, Y.; Shu, M.; Lin, Y.; Wang, Y.; Wang, R.; Hu, Y.; Lin, Z. Combined 3D-QSAR modeling and molecular docking study on azacycles CCR5 antagonists. *J. Mol. Struct.* **2013**, *1045*, 35–41.
18. Yin, L.; Hu, Q.; Hartmann, R.W. Tetrahydropyrroloquinolinone type dual inhibitors of aromatase/aldosterone synthase as a novel strategy for breast cancer patients with elevated cardiovascular risks. *J. Med. Chem.* **2013**, *56*, 460–470.
19. Gobbi, S.; Hu, Q.; Negri, M.; Zimmer, C.; Belluti, F.; Rampa, A.; Hartmann, R.; Bisi, A. Modulation of cytochromes P450 with xanthone-based molecules: From aromatase to aldosterone synthase and steroid 11 $\beta$ -hydroxylase inhibition. *J. Med. Chem.* **2013**, *56*, 1723–1729.
20. Gadhe, C.G.; Kothandan, G.; Cho, S.J. Binding site exploration of CCR5 using in silico methodologies: A 3D-QSAR approach. *Arch. Pharm. Res.* **2013**, *36*, 6–31.

21. Bhatt, H.G.; Patel, P.K. Pharmacophore modeling, virtual screening and 3D-QSAR studies of 5-tetrahydroquinolinylidene aminoguanidine derivatives as sodium hydrogen exchanger inhibitors. *Bioorganic Med. Chem. Lett.* **2012**, *22*, 3758–3765.
22. Ai, Y.; Wang, S.T.; Sun, P.H.; Song, F.J. Molecular modeling studies of 4,5-dihydro-1H-pyrazolo[4,3-h]quinazoline derivatives as potent CDK2/Cyclin A inhibitors using 3D-QSAR and docking. *Int. J. Mol. Sci.* **2010**, *11*, 3705–3724.
23. Ding, W.; Sun, M.; Luo, S.; Xu, T.; Cao, Y.; Yan, X.; Wang, Y. A 3D QSAR study of betulinic acid derivatives as anti-tumor agents using topomer CoMFA: Model building studies and experimental verification. *Molecules* **2013**, *18*, 10228–10241.
24. Almerico, A.M.; Tutone, M.; Pantano, L.; Lauria, A. A3 adenosine receptor: Homology modeling and 3D-QSAR studies. *J. Mol. Graph. Model.* **2013**, *42*, 60–72.
25. Balupuri, A.; Gadhe, C.G.; Balasubramanian, P.K.; Kothandan, G.; Cho, S.J. In silico study on indole derivatives as anti HIV-1 agents: A combined docking, molecular dynamics and 3D-QSAR study. *Arch. Pharmacol. Res.* **2013**, *37*, 1001–1015.
26. Parulekar, R.S.; Barage, S.H.; Jalkute, C.B.; Dhanavade, M.J.; Fandilolu, P.M.; Sonawane, K.D. Homology modeling, molecular docking and DNA binding studies of nucleotide excision repair UvrC protein from *M. tuberculosis*. *Protein J.* **2013**, *32*, 467–476.
27. Shen, J.; Zhang, W.; Fang, H.; Perkins, R.; Tong, W.; Hong, H. Homology modeling, molecular docking, and molecular dynamics simulations elucidated alpha-fetoprotein binding modes. *BMC Bioinform.* **2013**, *14* (Suppl. 14), doi:10.1186/1471-2105-14-S14-S6.
28. Yang, W.; Shu, M.; Wang, Y.; Wang, R.; Hu, Y.; Meng, L.; Lin, Z. 3D-QSAR and docking studies of 3-Pyridine heterocyclic derivatives as potent PI3K/mTOR inhibitors. *J. Mol. Struct.* **2013**, *1054–1055*, 107–116.
29. Richmond, N.J.; Abrams, C.A.; Wolohan, P.R.; Abrahamian, E.; Willett, P.; Clark, R.D. GALAHAD: 1. Pharmacophore identification by hypermolecular alignment of ligands in 3D. *J. Comput.-Aided Mol. Des.* **2006**, *20*, 567–587.
30. Liu, M.; Wu, Q.S.; Hu, W.X. Pharmacophore Screening on Piperidinecarboxamides Derivatives Based on GALAHAD and CoMFA Models. *Chin. J. Chem.* **2011**, *29*, 1075–1083.
31. Xiang, Y.; Hou, Z.; Zhang, Z. Pharmacophore and QSAR studies to design novel histone deacetylase 2 inhibitors. *Chem. Biol. Drug Des.* **2012**, *79*, 760–770.
32. Caballero, J. 3D-QSAR (CoMFA and CoMSIA) and pharmacophore (GALAHAD) studies on the differential inhibition of aldose reductase by flavonoid compounds. *J. Mol. Graph. Model.* **2010**, *29*, 363–371.
33. Arooj, M.; Thangapandian, S.; John, S.; Hwang, S.; Park, J.K.; Lee, K.W. 3D QSAR pharmacophore modeling, in silico screening, and density functional theory (DFT) approaches for identification of human chymase inhibitors. *Int. J. Mol. Sci.* **2011**, *12*, 9236–9264.
34. Amnerkar, N.D.; Bhusari, K.P. Synthesis, anticonvulsant activity and 3D-QSAR study of some prop-2-eneamido and 1-acetyl-pyrazolin derivatives of aminobenzothiazole. *Eur. J. Med. Chem.* **2010**, *45*, 149–159.
35. Cao, R.; Guan, X.; Shi, B.; Chen, Z.; Ren, Z.; Peng, W. Design, synthesis and 3D-QSAR of  $\beta$ -carboline derivatives as potent antitumor agents. *Eur. J. Med. Chem.* **2010**, *45*, 2503–2515.



36. Cvijetic, I.N.; Zizak, Z.P.; Stanojkovic, T.P.; Juranic, Z.D.; Terzic, N.; Opsenica, I.M.; Opsenica, D.M.; Jurani, I.O.; Drakuli, B.J. An alignment independent 3D QSAR study of the antiproliferative activity of 1,2,4,5-tetraoxanes. *Eur. J. Med. Chem.* **2010**, *45*, 4570–4577.
37. Debnath, U.; Verma, S.; Jain, S.; Katti, S.B.; Prabhakar, Y.S. Pyridones as NNRTIs against HIV-1 mutants: 3D-QSAR and protein informatics. *J. Comput.-Aided Mol. Des.* **2013**, *27*, 637–654.
38. Fernandez, D.; Ortega-Castro, J.; Frau, J. Human farnesyl pyrophosphate synthase inhibition by nitrogen bisphosphonates: A 3D-QSAR study. *J. Comput.-Aided Mol. Des.* **2013**, *27*, 739–754.
39. NCBI. National Center for Biotechnology Information Search database. Available online: <http://www.wip.ncbi.nlm.nih.gov/> (accessed on 3 October 2013).

*Sample Availability:* Samples of the all compounds are available from the authors.

© 2015 by the authors; licensee MDPI, Basel, Switzerland. This article is an open access article distributed under the terms and conditions of the Creative Commons Attribution license (<http://creativecommons.org/licenses/by/4.0/>).